Article:
Avrutin, E. A. and Ryvkin, B. S. (2017) Theory of direct and indirect effect of two-photon absorption on nonlinear optical losses in high power semiconductor lasers. Semiconductor science and technology. 015004. ISSN: 0268-1242

https://doi.org/10.1088/1361-6641/32/1/015004

Theory of direct and indirect effect of two photon absorption on nonlinear optical losses in high power semiconductor laser

E.A.Avrutin[1] and B.S. Ryvkin[2,3].

[1] *Dept of Electronics, University of York, York YO10 4LE, UK*

[2] *A.F.Ioffe Physico-Technical Institute, St.Petersburg 194021, Russia*

[3] *ITMO University, St.Petersburg 197101, Russia*

Abstract: the effect of the transverse laser structure on two-photon absorption (TPA) related effects in high-power diode lasers is analysed theoretically. The direct effect of TPA is found to depend significantly on the transverse waveguide structure, and predicted to be weaker in broad and asymmetric waveguide designs. The indirect effect of TPA, via carrier generation in the waveguide and free-carrier absorption, is analysed for the case of a symmetric laser waveguide and shown to be strongly dependent on the active layer position. With the active layer near the mode peak, the indirect effect is weaker than the direct effect due to the population of TPA-created carriers' being efficiently depleted by their diffusion and capture into the active layer, whereas for the active layer position strongly shifted towards the *p*-cladding, the indirect effect can become the dominant power limitation at very high currents. It is shown that for optimizing a laser design for pulsed high power operation, both TPA related effects and the inhomogeneous carrier accumulation in the waveguide caused by diffusive current need to be taken into account.

Introduction.

High power semiconductor lasers find numerous applications including, but not restricted to, optical communications (e.g. solid state laser and amplifier pumping), manufacturing industry, metrology and spectroscopy, optical radars, *etc.* (see e.g. [1] [2] for an overview). Achieving high output power and high efficiency is of paramount importance for many of these applications; this requires optimizing the laser structure, which in turn needs detailed understanding of physical phenomena that affect the laser performance at high power operation.

Since high-power diode lasers typically operate very high above threshold, the most important parameters for achieving high power output are the slope and injection efficiency of the laser, which need to be maximized. High slope efficiency, in its turn, requires low internal parasitic losses. All high-power lasers currently in use comprise a relatively broad Optical Confimenent Layer (OCL), sandwiched between *p*- and *n*- claddings and containing within it a thin (single or two-three Quantum Wells) Active Layer (AL). Then, the low parasitic losses at low to moderate pumping currents are ensured primarily by reducing the overlap of the transverse laser mode of the laser waveguide with the lossy *p*-cladding. A number of laser designs have been proposed to achieve this. Historically the first, and still the most widespread at the moment, is the design including a broadened (OCL thickness h > 1.5-2 μm), waveguide, symmetric or approximately symmetric in the sense that it has equal or similar refractive index steps at the boundaries between the OCL and both claddings; see for example [3-8]. The AL can be positioned either at or near the centre of the OCL as in [3-8], or near the *p*-cladding as in the case of Slab Coupled Optical Waveguide Lasers (SCOWL; see e.g. [9]). The broad OCL and a substantial refractive index step at the OCL-*p*-cladding interface ensure that most of the transverse mode power is contained within the OCL rather than the claddings, making for low internal losses, at least at low to moderate currents. The second low-loss laser waveguide design type, proposed and realised more recently by a number of

authors, e.g. [2], [10] [11] [12], builds partly on the earlier ideas of [13] and involves a *substantially asymmetric* waveguide with a refractive index step between the *n*-cladding and the OCL substantially smaller than that between the OCL and the *p*-cladding. Depending on the OCL thickness and the exact value of the refractive index steps, such a waveguide can be broad (in the sense that most of the optical power of the mode is localized in the OCL) or narrow (in the sense that most of the mode resides in the *n*-cladding [14]), but in either case the overlap with the *p*-cladding is kept low, ensuring low cladding-related optical loss. Recently, it was the broader asymmetric waveguide that found extensive use for both steady state operated [2] and gain-switched [10, 15] lasers.

It follows from our semi-analytical calculations [16],[17] and has been confirmed numerically and experimentally [2] that a structure with a strongly asymmetric position of the active layer (very near to the *p*-cladding) can be expected to keep its low-loss advantage, not just at low to moderate operating currents, but at high currents too. This is because such a structure minimizes the effect of spatially inhomogeneous accumulation of carriers in the OCL (mainly the *p*-side of it) at high currents due to the finite time of ambipolar-type carrier diffusion from the claddings across the OCL to the AL, and hence the free-carrier and intervalence band absorption by the carriers thus accumulated. Since the characteristic carrier density, which scales the optical loss, is in this case approximately proportional to the thickness of the *p*-OCL (the fraction of the OCL between the active layer and the *p*-cladding), this source of nonlinear loss is particularly efficiently minimized in laser designs with the position of the active layer shifted from the mode peak towards the *p*-cladding, particularly ones where the refractive index profile is also asymmetric [2, 11, 12] (the Extreme Double Asymmetric Structure, EDAS).

However, some sources of nonlinear loss at high currents clearly exist in *any* high-power laser design, symmetric or asymmetric, since even EDAS structures have been shown to exhibit power saturation at high currents, albeit at somewhat higher powers than symmetric structures [2] [12].

Several nonlinear mechanisms of such loss have been identified. Firstly, there is the relatively well known effect of free carrier absorption by the *homogeneously* distributed carrier population accumulated in the OCL due to the nonzero time of their capture from the OCL to the active layer and the nonzero rate of their thermal escape in the opposite direction [3] [18] [19]. Secondly, recently, it has been pointed out that given the high light intensities, the Two-Photon Absorption (TPA) within the waveguide, originally investigated for semiconductor optical *amplifiers* [20] [21], may become important in high-power lasers [22] [23].

The TPA effect, in its turn, involves in fact two effects: (i) the *direct* effect of nonlinear loss due to TPA and (ii) the *indirect* effect of the TPA serving as yet another source of carrier accumulation in the waveguide (OCL and claddings), adding to the optical losses due to free-carrier and intervalence band absorption. In [22], the indirect effect of the TPA was estimated as being, at least in some cases, more important than the direct one. The authors achieved good agreement with experiments for one particular, broad symmetric waveguide, laser design, using the bulk values of the Two-Photon Absorption, postulating a recombination time for the TPA-created free carriers in the OCL of the order of 10 ns (typical for nonradiative and spontaneous recombination in a weakly doped layer), and neglecting *all other* high-power loss mechanisms. The question of carrier transport, and therefore of the carrier distribution across the OCL, was not considered in those papers. It is therefore of interest to address the issue of the direct and indirect effects of the TPA for different waveguide structures (with transport taken fully into account), their relative importance compared to other loss mechanisms and to each other, and their dependence on the laser design. This is the purpose of this paper.

1. The laser designs considered.

We shall consider here representative examples of both of the main high-power laser designs discussed above. The first is a broadened, symmetric waveguide structure, intended for operation at λ=1.06 μm. The prototype version of the structure, shown in Figure 1a (solid line) alongside the corresponding modal power distribution, is a broad symmetric waveguide with h=2 μm and the AL positioned near the centre (slightly shifted towards the *p*-cladding to aid higher order mode discrimination [5] [24]); however in the simulations, both the OCL thickness and the AL position (the extreme case of the AL located near the OCL/*p*-cladding interface being shown in a dashed line as case 2 in Figure 1a) could be varied.

For comparison, we also consider a (broad) asymmetric structure, with the refractive index contrast at the OCL/*n*-cladding interface reduced to 0.01 and that at the OCL/*p*-cladding interface kept the same as in the symmetric structure. Shown in Figure 1b is the case of h=2 μm as in Figure 1b, though in simulations, again, an arbitrary thickness was considered. The main calculation parameters and their values are listed in Table 1.

2. The direct TPA effect.

The *local* two-photon absorption at any point in the laser waveguide can be written as

$$\alpha_{TPA}(x,z) = \beta_2(x) J(x,z), \tag{1}$$

with $\beta_2(x)$ [cm/W] the two-photon absorption coefficient, characterised by a (relatively weak) dependence on the transverse (vertical) coordinate x because of its dependence on the material composition, and $J(x,z)$ is the local light intensity which, assuming a single transverse mode, is

evaluated as $J(x,z)=\frac{P(z)}{w}\psi^2(x)$. Here $P(z)$ is the power at a given longitudinal position z, w is the laser stripe width (assuming a broad area laser, we consider the light distribution homogeneous in the lateral coordinate; a 2D generalisation for a single-mode stripe waveguide, along the lines presented in [21], is straightforward), and $\psi^2(x)$ is the laser modal intensity profile as shown in Figure 1 ($\psi(x)$ being the modal electric field distribution), normalised so that that $\int_{-\infty}^{\infty}\psi^2(x)dx=1$.

The *modal* TPA coefficient can then be calculated in the usual fashion of calculating waveguide absorption: $\alpha_{TPA}^{(\mathrm{mod})}(z)\approx\int_{-\infty}^{\infty}\alpha_{TPA}(x,z)\psi^2(x)dx$, giving

$$\alpha_{TPA}^{(\mathrm{mod})}(z)\approx\left(\frac{1}{w}\int_{-\infty}^{\infty}\beta_2(x)\psi^4(x)dx\right)P(z);$$

The calculation may be further simplified by noting that the dependence of the TPA coefficient on the refractive index step in the waveguide is of relatively little importance for both structures of interest: in the symmetric structure (and to a lesser extent in the asymmetric one as well), this is because of the relatively weak penetration of the field into the claddings for all important h values, and in the asymmetric structure, also because the composition, and thus the value of $\beta_2(x)$, in the OCL and the *n*-cladding (which between them contain nearly all the mode intensity) are very similar. Then, we can evaluate the TPA using the very simple formula

$$\alpha_{TPA}^{(\mathrm{mod})}\approx\left(\frac{\beta_2^{(OCL)}}{w}\int_{-\infty}^{\infty}\psi^4(x)dx\right)P=\beta_2^{(OCL)}\frac{P}{h_{TPA}w}; \qquad (2)$$

Here, $\beta_2^{(OCL)}$ is the TPA coefficient of the OCL (GaAs in our case) at the operating wavelength of interest (here, λ=1.06 μm), and

$$h_{TPA} = \left(\int_{-\infty}^{\infty} \psi^4(x)dx \right)^{-1}$$

is the transverse dimension characterising TPA in the waveguide. Eq. (2) is essentially a broad-area device version of the 2D integral given in [21].

Since in the waveguide structures of Figure 1, the effect of the active layer on the waveguiding is **very** weak, we can use the standard expression (see e.g. [25]) for the modal profile $\psi(x)$ in a three-layer slab waveguide

$$\psi(x) = \frac{1}{C_0}\cos(\kappa x - \varphi) \ , \quad 0<x<h \ \text{(OCL)} \tag{3a}$$

$$\psi(x) = \frac{1}{C_0}\cos\varphi \exp(\gamma_n x) \ , \ x<0 \quad (n\text{-cladding}) \tag{3b}$$

$$\psi(x) = \frac{1}{C_0}\cos(\kappa h - \varphi)\exp\left(-\gamma_p (x-h)\right) , \quad x> h \ (p\text{-cladding}) \tag{3c}$$

where $\kappa = \frac{2\pi}{\lambda}\sqrt{n_{OCL}^2 - n_0^2}$ is the transverse wave vector of the waveguide mode in the OCL, $\gamma_n = \frac{2\pi}{\lambda}\sqrt{n_0^2 - n_n^2}$ and $\gamma_p = \frac{2\pi}{\lambda}\sqrt{n_0^2 - n_p^2}$ are the decrements of decay into the *n*- and *p*-claddings, and $\varphi = \arctan\left(\frac{\gamma_n}{\kappa}\right)$. The values of κ, γ_n, and γ_p are calculated from the effective refractive index n_0 of the fundamental (TE) mode and the refractive indices n_{OCL}, n_p, n_n of the OCL, *p*- and *n*-cladding layers, respectively; see Appendix 1 for more detail. The normalisation constant is calculated as

$$C_o = \sqrt{\frac{h_{eff}}{2}}, \quad \text{where} \quad h_{eff} = h + \frac{1}{\gamma_n} + \frac{1}{\gamma_p}$$

characterises the transverse spread of the mode; for a mode well contained within the OCL, $h_{eff} \approx h$. The magnitude $h_{eff}/2$ is the effective mode size, defined (see e.g. [22]) as the width of a "top-hat" profile that contains the same total energy as the modal distribution $\psi^2(x)$ given the same amplitude ψ^2_{peak}. For a thin ($d_a << h$) active layer located at the peak of the mode, $h_{eff}/2$ also coincides with the ratio d_a/Γ_a ($\Gamma_a \approx \psi^2(l_a) d_a$ being the confinement factor, or the overlap of $\psi^2(x)$ with the active layer located at $x=l_a$), which is sometimes termed the *equivalent spot size* of the mode.

The formulas (3)a-c for $\psi(x)$ allow an explicit, if somewhat cumbersome, expression **(A1.7)** to be obtained for $h_{TPA} = \left(\int_{-\infty}^{\infty} \psi^4(x) dx \right)^{-1}$; see Appendix 1.

The result, obviously, depends on the specific design of a waveguide: n_{OCL}, n_p, n_n, and h.

Given a certain effective mode size $h_{\text{eff}}/2$, simple universal (not tied to a particular waveguide design) approximations for $\psi(x)$ can be constructed in order to obtain approximate estimates of waveguide properties, including the TPA parameter h_{TPA} . The first of these is a top-hat profile with an amplitude of $1/C_0 = \sqrt{2/h_{eff}}$ and thus a width of $h_{eff}/2$, which gives an estimate $h_{TPA}^{(top-hat)} = h_{eff}/2$. The second (a one-dimensional equivalent of a two-dimensional approximation used in [21] for a narrow stripe waveguide with a single transverse and lateral mode) is a Gaussian profile with the same amplitude (which, given the normalisation $\int_{-\infty}^{\infty} \psi^2(x) dx = 1$, ensures the same effective mode size). This results in an estimate $h_{TPA}^{(\text{Gauss})} = \sqrt{2} h_{eff}/2$.

Shown in Figure 2, as functions of h, are the values of the integral $\int_{-\infty}^{\infty} \psi^4(x)dx = 1/h_{TPA}$,which scales the absorption coefficient $\alpha_{TPA}^{(\mathrm{mod})}$, for the symmetric (a) and asymmetric (b) waveguide designs, calculated both accurately and using the top-hat and, in the case of a symmetric waveguide, Gaussian approximations for the same h_{eff}. It is seen from the figure that, whilst for narrow waveguides the accurate evaluation is desirable, for broader ones (in excess of about a micrometer), the Gaussian approximation gives a very accurate estimate.

Interestingly, the TPA in a broad symmetric waveguide (with a typical value of h~2 μm) can be expected to be significantly greater than in an asymmetric waveguide at the same power and with a similar waveguide thickness, because the asymmetric waveguide mode has a larger effective size.

We note that a formalism equivalent but alternative to Eq. (2), used in [21] and [22] to describe the TPA in a laser or amplifier, is to introduce the effective modal light intensity, or flux, J_{mod}, and express the nonlinear loss coefficient in a form formally identical to the bulk expression (1): $\alpha_{TPA}^{(\mathrm{mod})}(z) \approx \beta_2^{(\mathrm{mod})} J_{\mathrm{mod}}$, with an effective modal TPA coefficient $\beta_2^{(\mathrm{mod})}$. However, in this case one needs to take some care about the way the effective flux, and thus the effective modal TPA coefficient, are defined. Using only the waveguide mode parameters, J_{mod} can be defined as $J_{\mathrm{mod}}=P/A_{\mathrm{mod}}$ as in [21], where A_{mod} is the effective modal cross-section (in the case of a broad-area slab waveguide, $A_{\mathrm{mod}}=h_{eff}w/2$ in our notations; the two-dimensional generalisation for a single-mode *stripe* waveguide is given in [21]). With such notations, from (2), $\beta_2^{(\mathrm{mod})} = \beta_2^{(OCL)} h_{eff} / (2h_{TPA})$, and in the Gaussian approximation, which, as mentioned above, is very accurate for broad symmetric waveguides, simply $\beta_2^{(\mathrm{mod})} \approx \sqrt{2}\beta_2^{(OCL)} / 2$. The authors of [22] used a different, generally speaking, definition of the effective modal flux, performing their calculations, instead of J_{mod} as determined above, for a flux $J_a=P\Gamma_a/(wd_a)$ seen by the *active layer* and thus directly scaling

the stimulated recombination rate $\left(\frac{dN_a}{dt}\right)_{stim} = -g\frac{J_a}{\hbar\omega}$ of carriers in the AL (g being the gain and N_a, the AL carrier density). Note that $J_a = J_{\mathrm{mod}}$ if and only if the AL is located at the mode peak. In terms of the flux J_a, one can express the absorption coefficient formally as $\alpha_{TPA}^{(\mathrm{mod})} \approx \beta_2^{(\mathrm{mod,a})} J_a$, where the equivalent modal TPA coefficient is calculated as $\beta_2^{(\mathrm{mod,a})} = \beta_2^{(OCL)} d_a / (2\Gamma_a h_{TPA})$ and is thus, generally speaking, a function of the AL position, even though the actual absorption $\alpha_{TPA}^{(\mathrm{mod})}$ is not, if $d_a << h$. In [22], an approximation $\alpha_{TPA}^{(\mathrm{mod})} \approx \beta_2^{(\mathrm{OCL})} J_a$ was used; without knowing the waveguide structure and the position of the OCL in the waveguide used in [22], one cannot compare this approximation with the more accurate calculation using $\beta_2^{(\mathrm{mod,a})}$. We believe the expression (2) is thus the most straightforward and unambiguous representation of the nonlinear properties of a laser waveguide, since it relates the nonlinear absorption to local *power*, a parameter independent on the modal structure.

3. The indirect TPA effect: TPA-created carriers.

The TPA-created carriers are generated throughout the OCL and removed, firstly, through radiative and nonradiative recombination, and, secondly, through transport and subsequent capture into the active layer. In analysing the transport, we follow the previous work [16, 17, 26] in assuming *detailed quasineutrality*. In an undoped or very weakly doped OCL considered here, this means identical electron and hole densities $N_e \approx N_h \approx N$ throughout the bulk of the OCL (that is, in the whole of the OCL with the exception of a narrow region around the active layer). The approximation is in excellent agreement with numerical simulations in the absence of TPA, and can be confidently expected to hold in its presence as well, seeing that TPA creates electron-hole *pairs* at each point. Note that the second of the approximations made in [16, 17, 26], that of the absence of the electron current in the entire p-OCL (which is defined as the area $l_a < x < h$) and the hole current in the entire n-OCL ($0 < x < l_a$), is not made here since it is incompatible with the presence of carrier generation

and/or recombination. With quasineutrality postulated, the carrier transport is described by the standard ambipolar diffusion equation (including z dependence because of the variation of power along the resonator length):

$$D_a \frac{\partial^2 N}{\partial x^2} + G(x,z) - R(N(x,z)) = 0 \tag{4}$$

Here, $D_a = \frac{2D_e D_h}{D_e + D_h}$ is the ambipolar diffusion coefficient, D_e and D_h being the electron and hole diffusion coefficients in the OCL material, diffusion in the longitudinal direction z is omitted due to the relatively long distance scales involved, and the generation term is given by the TPA rate:

$$G(x,z) = \frac{\beta_2(x)}{\hbar\omega}\left(\frac{P(z)}{w}\right)^2 \psi^4(x) \tag{5}$$

The recombination rate R should, in principle, include both the bimolecular radiative and linear nonradiative recombination terms as in [26]. However, as was shown previously [26], in the absence of TPA the recombination term is only important with very high (in excess of 10^{18} cm^{-3}) OCL carrier densities and/or very broad OCL (~3-4 μm). Here we consider somewhat narrower OCLs, and are primarily concerned with GaAs/AlGaAs materials where D_a is a few times greater than in InGaAsP quaternaries treated in [26], so it can be confidently expected that with TPA present, transport and subsequent capture should remain a more efficient OCL carrier dissipation route than recombination. Therefore in this paper we shall only consider transport, not recombination, and set R=0 in the first approximation. If necessary, it is relatively straightforward to include recombination in the second approximation using an approximate iterative procedure [26] having first calculated the carrier distribution with R=0; *linear* recombination could even be included exactly from the start but is unlikely to be the dominating recombination mechanism due to high material quality which can be expected in the weakly doped OCL of a high power laser.

The boundary conditions for Eq. (4) are taken to be approximately the same as in the absence of TPA [16, 17, 26] : at the interfaces with injectors (claddings), the current is carried almost entirely (entirely, barring current leakage) by electrons at the OCL-*n*-cladding interface x=0 and by holes at the OCL-*p*-cladding interface $x=h$:

$$\left.\frac{\partial N}{\partial x}\right|_{x=0} = -\frac{\eta_{lh} j}{2D_e}; \quad \left.\frac{\partial N}{\partial x}\right|_{x=h} = \frac{\eta_{le} j}{2D_h}; \tag{6}$$

Here, $\eta_{lh} = \eta_{lh}(j)$ and $\eta_{le} = \eta_{le}(j)$ are efficiency coefficients describing the leakage of hole current into the *n*-cladding and of electron current into the *p*-cladding correspondingly; they can be estimated as described in [18] [27] and are equal to one in the absence of leakage. Note that the analysis below is restricted to situations when the leakage is not strong (η_{lh}, η_{le} are close to one) which is nearly all situations of practical interest in GaAs/AlGaAs lasers, particularly for the strongly guiding structure of Figure 1a.

At the OCL (more accurately, at a very small distance away from it, where the bulk quasineutrality begins to hold, but this distance is much smaller than h so can be neglected), we have

$$N\big|_{x=l_a+} = N\big|_{x=l_a-} = N_b \tag{7}$$

, where N_b is the background carrier density determined by the balance of carrier capture from the OCL into the AL and the thermally activated escape in the opposite direction, as in previous papers. Strictly speaking, both boundary conditions are slightly affected by the presence of the TPA: the conditions (6) because η_{lh} and η_{le} are affected by the TPA in the claddings themselves, and the conditions (7) because TPA adds some extra carriers to the balance of capture and escape – however both effects can be estimated to be rather weak.

In the absence of bimolecular recombination, Eq. (4) is linear in N, so its solution with the boundary conditions (6) and (7) can be conveniently separated into, firstly, the TPA-independent part

including the spatially homogeneous background N_b and the spatially inhomogeneous part $\Delta N_j(x)$ caused only by current flow and identical in its form to the results of [17] [16], and secondly, the TPA-dependent part $\Delta N_{TPA}(x,z)$ proportional to P^2:

$$N(x,z) = N_b + \Delta N_j(x) + \Delta N_{TPA}(x,z) \tag{8}$$

With R=0, the current contribution is the same as derived in [16, 17, 26]:

$$\begin{aligned} \Delta N_j(x) &= \frac{\eta_{lh} j}{2D_e}\left(l_a - x\right) \;; \quad 0 < x < l_a \\ \Delta N_j(x) &= \frac{\eta_{le} j}{2D_h}\left(x - l_a\right); \quad l_a < x < h \end{aligned} \tag{9}$$

The spatially homogeneous background N_b can be estimated as

$$N_b \approx \frac{j}{ed_a}\tau_{cap} + N_{bT} \tag{10}$$

where τ_{cap} is the characteristic time of carrier capture into the QW AL which for the carrier density values small enough to keep the quasi Fermi levels deep in the well has been calculated (see e.g. [28]) as τ_{cap} ~ (100-200) fs; d_a is the AL thickness (taken as 10 nm). The term N_{bT} describes the thermal escape from the AL into the OCL. Under room temperature operation, which is the subject of this paper, it is usually weak, but can easily become dominant at elevated temperatures which are characteristic of true CW high power operation.

The TPA-generated carrier density is obtained by integrating the generation term (5) twice with the boundary conditions $\left.\frac{\partial \Delta N_{TPA}}{\partial x}\right|_{x=0} = \left.\frac{\partial \Delta N_{TPA}}{\partial x}\right|_{x=h} = 0; \quad \Delta N_{TPA}\big|_{x=l_a+} = \Delta N_{TPA}\big|_{x=l_a-} = 0$

The integration itself is trivial if somewhat cumbersome; the explicit resulting expressions are given in the Appendix 1.

From the carrier distributions, since both the carrier density accumulation and the waveguide mode in the laser structures are localised in the OCL (as illustrated in Figure 3) under the conditions considered here, the corresponding contributions to the internal absorption are calculated as

$$\alpha_j^{(FC)}(z) \approx \left(\sigma_e + \sigma_h\right) \int_0^h \left[N_b - N_{bT} + \Delta N_j\left(x, z\right) \right] \psi^2(x) dx \tag{11}$$

and

$$\alpha_{TPA}^{(FC)}(z) \approx \left(\sigma_e + \sigma_h\right) \int_0^h \Delta N_{TPA}\left(x, z\right) \psi^2(x) dx \ , \tag{12}$$

where σ_e, σ_h are the free-electron and free-hole absorption cross-sections, respectively.

Note that in (11), we have included the contributions from both ΔN_j and the current-dependent part of N_b since both are scaled by the current density *j*.

The relative magnitudes of ΔN_j and ΔN_{TPA} are somewhat current dependent since ΔN_j is proportional to the current density *j* and ΔN_{TPA}, as already noted in [22] [23], to the *square* of power and hence depends on *j* superlinearly, if not exactly quadratically, therefore its relative effect compared to ΔN_j increases with current.

To calculate the power *P*(*j*) needed for evaluation of ΔN_{TPA}, we used a self-consistent procedure including all the nonlinear loss mechanisms discussed here. Within this procedure, the power *P* as function of current *i* (or current density *j*=*i*/*wL*, recalculated using the cavity length *L*=3 mm, width *w*=100 μm) is determined from a transcendental equation

$$P(i) = \frac{\hbar\omega}{e} \frac{\alpha_{out}}{\alpha_{out} + \alpha_{in}(i, P(i))} \left(i - i_{th}\right) \tag{13}$$

where the output loss $\alpha_{out} = \frac{1}{2L} \ln \frac{1}{R_{HR} R_{AR}}$ was calculated assuming the high-reflectance and antireflectance coated facet reflectances $R_{HR} \approx 1$, R_{AR}=0.05. The threshold current value i_{th} did not

affect the results much, given the range of currents $i>>i_{th}$. The internal loss was calculated as a sum of all contributions

$$\alpha_{in}(i,P(i)) \approx \alpha_{in}^{(\text{built}-\text{in})} + \alpha_{j}^{(\text{FC})}(i) + \alpha_{TPA}^{(\text{FC})}(P(i)) + \alpha_{TPA}^{(\text{mod})}(P(i)) \tag{14}$$

In this equation, the constant built-in absorption $\alpha_{in}^{(\text{built}-\text{in})}$ included the effects of cladding doping, structure imperfections, and free carrier absorption by the thermally escaping OCL carriers (the N_{bT} term in (10)); the value for it was taken as 0.4 cm^{-1} [24]. We treat the case of pulsed (quasi-CW) operation so the thermal roll-over is not considered in the simulations, and the value of N_{bT} can be approximately taken as constant. For the free-carrier absorption cross-sections, we used σ_e=3×10^{-18} cm^2, σ_h=1×10^{-17} cm^2 as in previous work [17].

Figure 3 shows the distribution of the different carrier density contributions in the structure of Figure 1a for both positions of the active layer shown in the figure (with the waveguide structure and the intensity distribution also repeated for reference) for the value of j=50 kA/cm^2, which towards the upper limit of what is realistically achievable. As the paper addresses the pulsed operation regime, all the calculations were performed with room-temperature parameters, e.g. we took D_e=200 cm^2/s; D_h=10 cm^2/s. As implied by the form of (13), in this part of the work, to present a clear physical picture concentrating on the effects of TPA and carrier accumulation, we used a longitudinally lumped model, not taking into account photon density distribution $P(z)$ along the cavity and thus longitudinal spatial hole burning (LSHB). We can however note in passing that even in the case of LSHB present, there would always be a certain cross-section of the laser cavity (a certain value of z) for which the local value of power, and hence the carrier density distribution, would correspond to that presented in Figure 3.

It is clear from Figure 3 that, in addition to current, both the form of the carrier density distribution and the relative magnitudes of ΔN_j and ΔN_{TPA} are critically dependent on the position of the active

layer with respect to the *p*-cladding. If the active layer is positioned near the centre of the OCL, the slow ambipolar diffusion in the broad *p*-OCL leads to very significant values of ΔN_j, with $\Delta N_j\big|_{x=h}$ reaching values of the order of 10^{18} cm^{-3}, as already discussed in earlier papers [16, 17, 26]. Conversely, the TPA-created carrier density is in this case efficiently depleted, due to the fact that the carrier drain due to the capture into the AL is spatially very close to the point of the maximum TPA generation (the modal peak).

As the AL is shifted towards the *p*-cladding (l_a is increased), the *p*-OCL becomes narrower and the *n*-OCL (in which the slope of $\Delta N_j(x)$ as described by Eq. (9) is much lower than in the *p*-OCL since $D_e >> D_h$), correspondingly wider; therefore overall, the effect of ΔN_j in the waveguide is significantly reduced. Meanwhile, the TPA-created carriers become less efficiently depleted with an increased l_a as their generation and drain become increasingly separated in space. This leads to a substantial increase in ΔN_{TPA} which at the very high current shown in the figure actually exceeds ΔN_j throughout the *n*-OCL (in the *p*-OCL, ΔN_{TPA} conversely becomes very low, but as the *p*-OCL is now much narrower than the *n*-OCL, this has less effect on the absorption). It has to be noted however that even in the case of the AL near the *p*-cladding, the effect of the TPA-created carriers is substantially smaller than that used in the papers [22] [23] where the capture of the TPA-created carriers into the AL (and thus the nature of their spatial distribution) was ignored, as was the current-generated carrier population, both uniform and nonuniform, and carrier density was (implicitly) determined by the carrier recombination time in the OCL.

As can be expected, the tendencies discussed above are reflected in the dependence of the various contributions to the internal loss on the active layer position l_a, which is shown in Figure 4 for the current density value of j=50 kA/cm^2. As discussed above, $\alpha_j^{(FC)}$ decreases as the AL is shifted towards the *p*-cladding (l_a increases), whereas $\alpha_{TPA}^{(FC)}$ increases. The other contributions (the built-

in losses and the direct TPA contribution) are virtually independent of l_a (the weak parametric dependence of $\alpha_{TPA}^{(\mathrm{mod})}$ on l_a is due to the dependence of the power on l_a in the self-consistent calculation). There is thus an optimal AL position that minimises the losses for a given current density value, though the optimum is neither sharp nor very pronounced – the combination of $\alpha_j^{(FC)}$ and $\alpha_{TPA}^{(FC)}$ with their opposite dependence on l_a leads to the dependence of the total loss on the active layer position being much weaker than that of either $\alpha_j^{(FC)}$ or $\alpha_{TPA}^{(FC)}$ on their own.

Figure 5 shows the l_a dependence of total losses (Figure 5a) and the corresponding power values (Figure 5b) for three current density values. The minimum of loss (or maximum of power) discussed above is seen at all current values studied; its position shifts somewhat away from the *p*-cladding and towards the centre of the OCL as the current is increased, though only slightly, because of the sublinear dependence $P(j)$.

As in the case of Figure 3, to calculate $P(j)$ in all subsequent figures we mainly used a self-consistent procedure including all the nonlinear loss mechanisms discussed here, but using the lumped approximation (13) ignoring the longitudinal power variation $P(z)$; those are the results shown as lines. We have verified that for the values of the laser cavity geometry parameters L and w and antireflection and high-reflection coated facet reflectance coefficients R_{AR}, R_{HR} (often used in practice, see e.g. [5, 24]) used in the calculations, the lumped model provides good accuracy, not just qualitatively, but quantitatively as well. As an illustration, Figure 5 includes, in addition to the lines, also results calculated for the three representative active layer positions (l_a=1.17 μm near the OCL centre and l_a=1.8 μm near the *p*-cladding as in Figure 1a, and in addition l_a=1.45 μm near the optimum) using a *distributed* model similar to those of [22, 23, 29]) with power P, and hence $\alpha_{TPA}^{(FC)}$ and $\alpha_{TPA}^{(\mathrm{mod})}$, calculated locally, as functions of z. These are represented as filled dots in Figure 5b. Comparison of these results to those obtained using the lumped model indicates that, while LSHB

slightly modifies the calculated power, the modification is small (about 4% at the highest current) and does not affect the dependence of power on l_a , including the position of the optimum. More detailed analysis, including treating laser structures with longer cavities and/or lower R_{AR}, where LSHB can be somewhat more important [30], is reserved for further work.

The results imply therefore that there is a design of the laser waveguide (the active layer position l_a) that would be near enough to the optimal position for high-power operation in a broad range of currents.

This is confirmed by Figure 6 which shows calculated losses as function of *current* with the active layer position as a parameter; it is seen that the loss value for l_a=1.45 µm, which is close to optimal for all values of *j*, stays below the loss calculated for the two "extreme" positions (near the centre of the waveguide and near the *p*-cladding) within the whole range of current densities.

Finally, Figure 7 shows the light-current curves calculated for various active layer positions and different effects taken into account. The dashed line in all graphs is a linear curve taking into account only built-in losses. As can be expected from Figures 4-6, for the near-central position of the active layer (l_a=1.17 µm, Figure 7a) as well as for l_a=1.45 µm, (Figure 7b) the main deviation of the light-current curve from the linear approximation is due to carrier build-up because of current ($\alpha_j^{(FC)}$), whereas for the case of the AL near the *p*-cladding (l_a=1.8 µm, Figure 7c), the carrier accumulation due to TPA and the corresponding loss mechanism $\alpha_{TPA}^{(FC)}$ are at least as important as $\alpha_j^{(FC)}$. Also as implied by Figure 6, the power output is the highest, of the three cases presented, for the near-optimum active layer location (l_a=1.45 µm).

It has to be noted that Figures 6-7 were calculated assuming that the laser in all cases operates in a single, fundamental transverse mode at all currents. For the case of l_a=1.17 µm, this can indeed be confidently expected, because this position is optimised for best modal discrimination [24]. For the

other two positions, reliable single-mode operation cannot be guaranteed and operation in the second order mode, at least for lower currents, as discussed in [31], cannot be ruled out. In this case, *double* asymmetry of the laser structure, with both the active layer position and the refractive index profile (as in Figure 1b) being asymmetric, is necessary to ensure reliable fundamental mode operation. Detailed optimisation is reserved for future work, but it can be expected that the optimum position of the active layer will be not too different from the one obtained for the symmetric waveguide.

4. Conclusions.

We have developed an efficient semi-analytical approach to analyse the direct ($\alpha_{TPA}^{(\mathrm{mod})}$) and indirect ($\alpha_{TPA}^{(FC)}$, due to free carrier absorption by TPA-created carriers) TPA contributions to optical losses in high power laser diodes as functions of laser structure and operating conditions, taking into account the structure geometry and the effects of carrier transport which we identified as the main mechanism of drain for TPA-created carriers.

Both of the TPA effects were found to be less important than the optical loss $\alpha_j^{(FC)}$ due to current-induced inhomogeneous carrier accumulation for broad waveguides with the active layer positioned approximately symmetrically in an undoped OCL. We found however that the TPA became more important for those structures where the AL is located nearer the *p*-cladding. In this latter case, the indirect TPA effect was shown to become more important than both the direct one and the effect of current induced carrier accumulation in determining the output power: $\alpha_{TPA}^{(FC)} > \alpha_{TPA}^{(\mathrm{mod})}$; $\alpha_{TPA}^{(FC)} > \alpha_j^{(FC)}$, which agrees qualitatively with the experimental findings for SCOW amplifiers [20]. Therefore, in general, both $\alpha_j^{(FC)}$ and the TPA effects need to be taken into account when optimising the laser structure for high power pulsed operation. Indeed, the combination of the different dependences of $\alpha_{TPA}^{(FC)}$ and $\alpha_j^{(FC)}$ on the active layer position l_a was shown to lead to the existence of an optimum

active layer position l_a, located between the centre of the OCL and the *p*-cladding and relatively weakly dependent on current.

In its present form, the analysis is restricted to laser designs where most of the optical mode intensity resides in the OCL; however, we believe the findings are generic enough to be important for high power laser optimisation.

Appendix 1. Expressions for the waveguide mode and the carrier density distribution.

In the simulations, the modal profile $\psi(x)$ (as shown in figures), and the modal refractive index n_0 were obtained for the sake of generality from a multilayer mode solver including the waveguiding properties of the active layer, but we verified that the results were very close to those obtained in a simple three-layer slab waveguide model, since $d_a << h$. In that model, the expressions for $\psi(x)$ can be taken from Ref. [25] and is given by Eq. (3)a-c in the main text.

The value of n_0 is found from the usual transcendental equation

$$\kappa h = \arctan\left(\frac{\gamma_n}{\kappa}\right) + \arctan\left(\frac{\gamma_p}{\kappa}\right) \tag{A1.1}$$

where $\kappa, \gamma_n, \gamma_p$ are functions of n_0 as described in the main text.

This form of $\psi(x)$ results in the expression for the TPA parameter $\int_{-\infty}^{\infty} \psi^4(x)dx = 1/h_{TPA}$ in the form

$$h_{TPA}^{-1} = \frac{1}{h_{eff}^2}\left\{\frac{3}{2}h + \frac{1}{\kappa}\sin\left(2(\kappa h - \varphi)\right) + \frac{1}{\kappa}\sin\varphi + \frac{1}{8\kappa}\sin\left(4(\kappa h - \varphi)\right) + \frac{1}{8\kappa}\sin 4\varphi + \frac{\cos^4\varphi}{\gamma_n} + \frac{\cos^4(\kappa h - \varphi)}{\gamma_p}\right\} \tag{A1.2}$$

For the TPA-induced carrier distribution, the double integration of the generation term with the zero boundary conditions as in the main text gives for the n-OCL ($0<x<l_a$):

$$\Delta N_{TPA}(x,z) = \frac{B(z)}{8D_a}\left[C_{2n} + C_{1n}x - \frac{3}{2}x^2 + \frac{1}{16\kappa^2}\cos\left(4(\kappa x - \varphi)\right) + \frac{1}{\kappa^2}\cos\left(2(\kappa x - \varphi)\right)\right] \tag{A1.3}$$

with

$$C_{1n} = -\frac{1}{4\kappa}\left(8\sin 2\varphi + \sin 4\varphi\right); \tag{A1.4a}$$

$$C_{2n} = \frac{3}{2}l_a^2 - C_{1n}l_a - \frac{1}{16\kappa^2}\cos\left(4(\kappa l_a - \varphi)\right) - \frac{1}{\kappa^2}\cos\left(2(\kappa l_a - \varphi)\right) \tag{A1.4b}$$

For the *p*-OCL ($l_a < x < h$):

$$\Delta N_{TPA}(x,z) = \frac{B(z)}{8D_a}\left[C_{2p} + C_{1p}x - \frac{3}{2}x^2 + \frac{1}{16\kappa^2}\cos\left(4(\kappa x - \varphi)\right) + \frac{1}{\kappa^2}\cos\left(2(\kappa x - \varphi)\right)\right] \tag{A1.5}$$

with

$$C_{1p} = 3h + \frac{2}{\kappa}\sin\left(2(\kappa h - \varphi)\right) + \frac{1}{4\kappa}\sin\left(4(\kappa h - \varphi)\right) \tag{A1.6a}$$

$$C_{2p} = \frac{3}{2}l_a^2 - C_{1p}l_a - \frac{1}{16\kappa^2}\cos\left(4(\kappa l_a - \varphi)\right) - \frac{1}{\kappa^2}\cos\left(2(\kappa l_a - \varphi)\right), \tag{A1.6b}$$

where in all expressions,

$$B(z) = \frac{4\beta_2(x)}{\hbar\omega}\left(\frac{P(z)}{h_{eff}w}\right)^2 \tag{A1.7}$$

Figure captions

Figure 1. Schematic of the structures evaluated and the corresponding intensity distributions in the (fundamental) waveguide mode: (a) the symmetric waveguide (with two active layer positions shown approximately indicating the range studied); (b) the asymmetric waveguide

Figure 2. The waveguide (OCL) thickness dependence of the TPA parameter for symmetric (a) and asymmetric (b) waveguides shown in Figure 1. Solid: exact calculation, dashed - Gaussian approximation of the transverse mode profile, dash-dotted - top-hat approximation.

Figure 3. Calculated spatial distributions of t contributions to the carrier density in the OCL due to current (a) and TPA(b). Solid: l_a=1.17 μm; dashed: l_a=1.8 μm. The waveguide profile and modal distribution (for l_a=1.17 μm) shown for reference.

Figure 4. Dependence of the total modal absorption and its constituent parts on the active layer position l_a for the waveguide of Figure 1a and the current density of j= 50 A/cm^2 (current i=150 A)

Figure 5. Dependence of the total modal absorption (a) and the corresponding laser output power (b) on the active layer position l_a for the waveguide of Figure 1a and three values of carrier density. Solid lines are calculated in the lumped laser model, dots in a distributed model taking into account Longitudinal Spatial Hole Burning.

Figure 6. Carrier density dependences of the total modal absorption in the waveguide of Figure 1a and for the three positions of the active layer shown as dots in Figure 5b. Cavity length L= 3 mm, stripe width w = 100 μm

Figure 7. Output power vs current curves calculated for a laser of Figure 1a, with the cavity length L= 3 mm and stripe width w = 100 μm, for the three positions of the active layer shown in Figures 5b and 6: l_a=1.17 μm (a), l_a=1.45 μm (b), l_a=1.8 μm (c), taking into account different internal loss

contributions: (1) $\alpha_{in}^{(\text{built-in})}$ only; (2) $\alpha_{in}^{(\text{built-in})} + \alpha_{j}^{(\text{FC})}$; (3) $\alpha_{in}^{(\text{built-in})} + \alpha_{j}^{(\text{FC})} + \alpha_{TPA}^{(\text{mod})}$; (4) all nonlinear effects: $\alpha_{in} = \alpha_{in}^{(\text{built-in})} + \alpha_{j}^{(\text{FC})} + \alpha_{TPA}^{(\text{FC})} + \alpha_{TPA}^{(\text{mod})}$

Table 1. The main source parameters and their values.

symbol	parameter	Value
$\hbar\omega$	photon energy	1.17 eV (λ=1.06 μm)
n_{OCL}	OCL refractive index	3.474
n_n	*n*-cladding refractive index	3.464 (asymmetric) 3.300 (symmetric)
n_p	*p*-cladding refractive index	3.300
$\beta_2^{(OCL)}$	TPA coefficient in the OCL	2×10^{-8} cm/W
L	cavity length	3 mm
w	stripe width	100 μm
R_{AR}	AR coated facet reflectance	0.05
R_{HR}	HR coated facet reflectance	≈1
h	waveguide thickness	2 μm (Section 3)
σ_e	free-electron absorption cross section	3×10^{-18} cm^2
σ_h	Free-hole absorption /IVBA cross-section	1×10^{-17} cm^2
D_e	electron diffusion coefficient	200 cm^2/s
D_h	hole diffusion coefficient	10 cm^2/s
$\alpha_{built\text{-}in}$	built-in modal absorption coefficient	0.4 cm^{-1}

Figures.

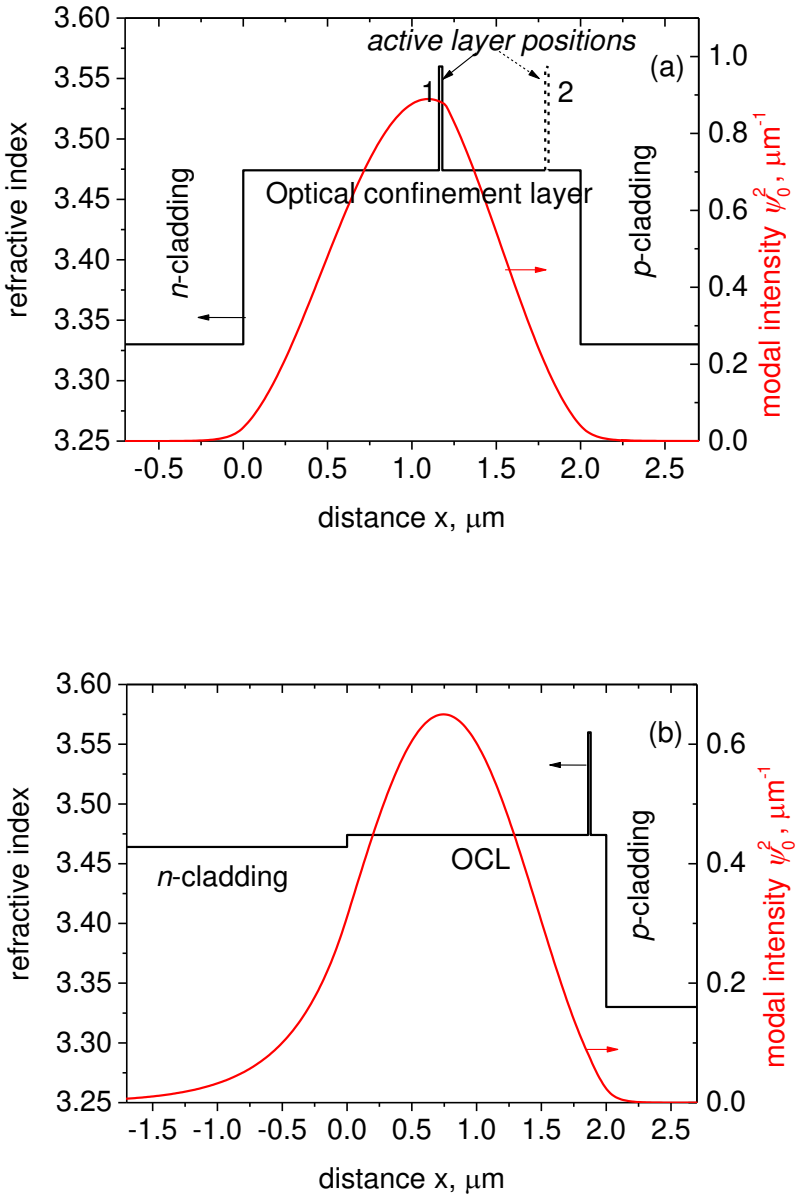

Figure 1.

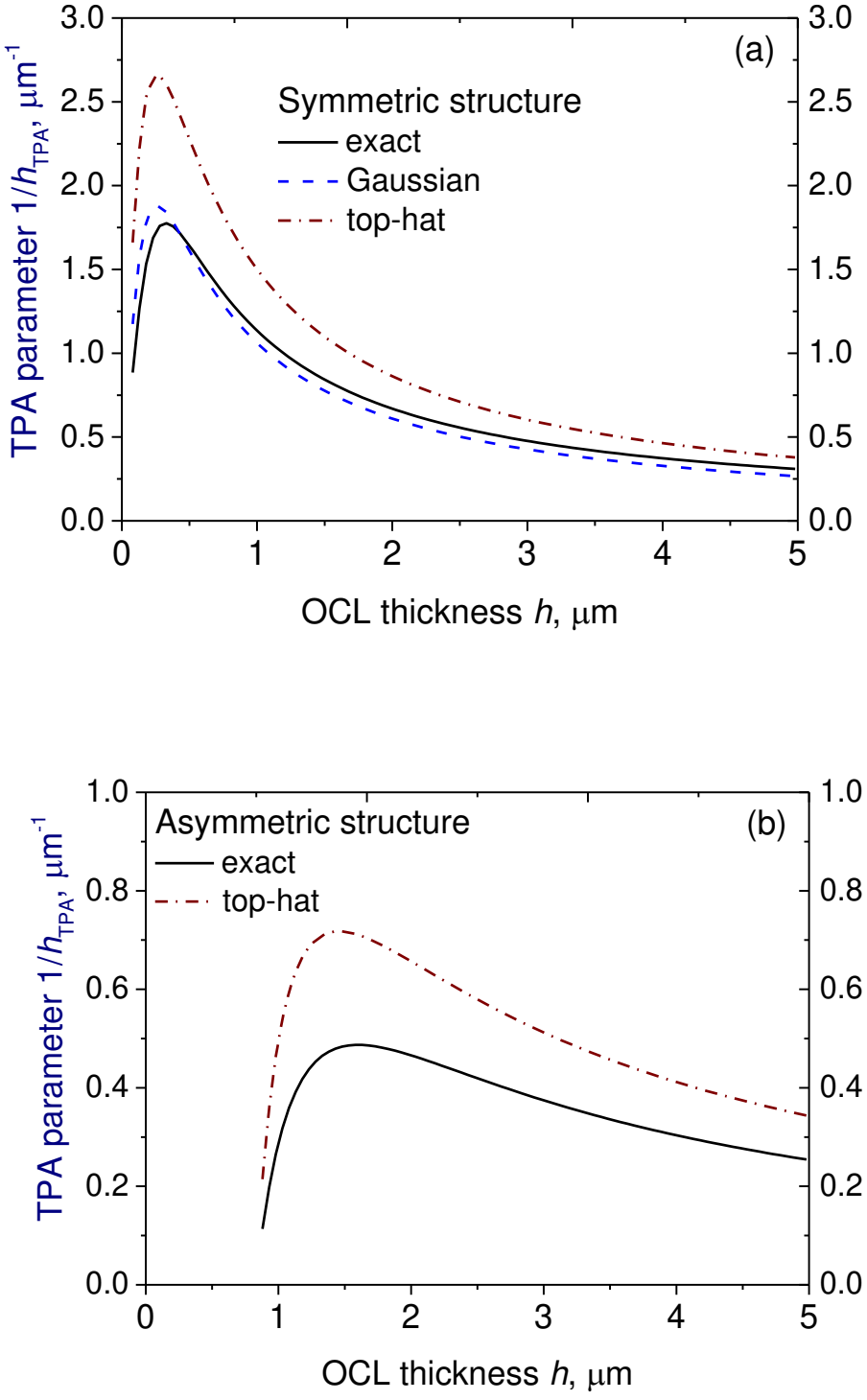
(a)
Symmetric structure
exact
Gaussian
top-hat
TPA parameter 1/h_{TPA}, μm^{-1}
OCL thickness h, μm
(b)
Asymmetric structure
exact
top-hat
TPA parameter 1/h_{TPA}, μm^{-1}
OCL thickness h, μm

Figure 2.

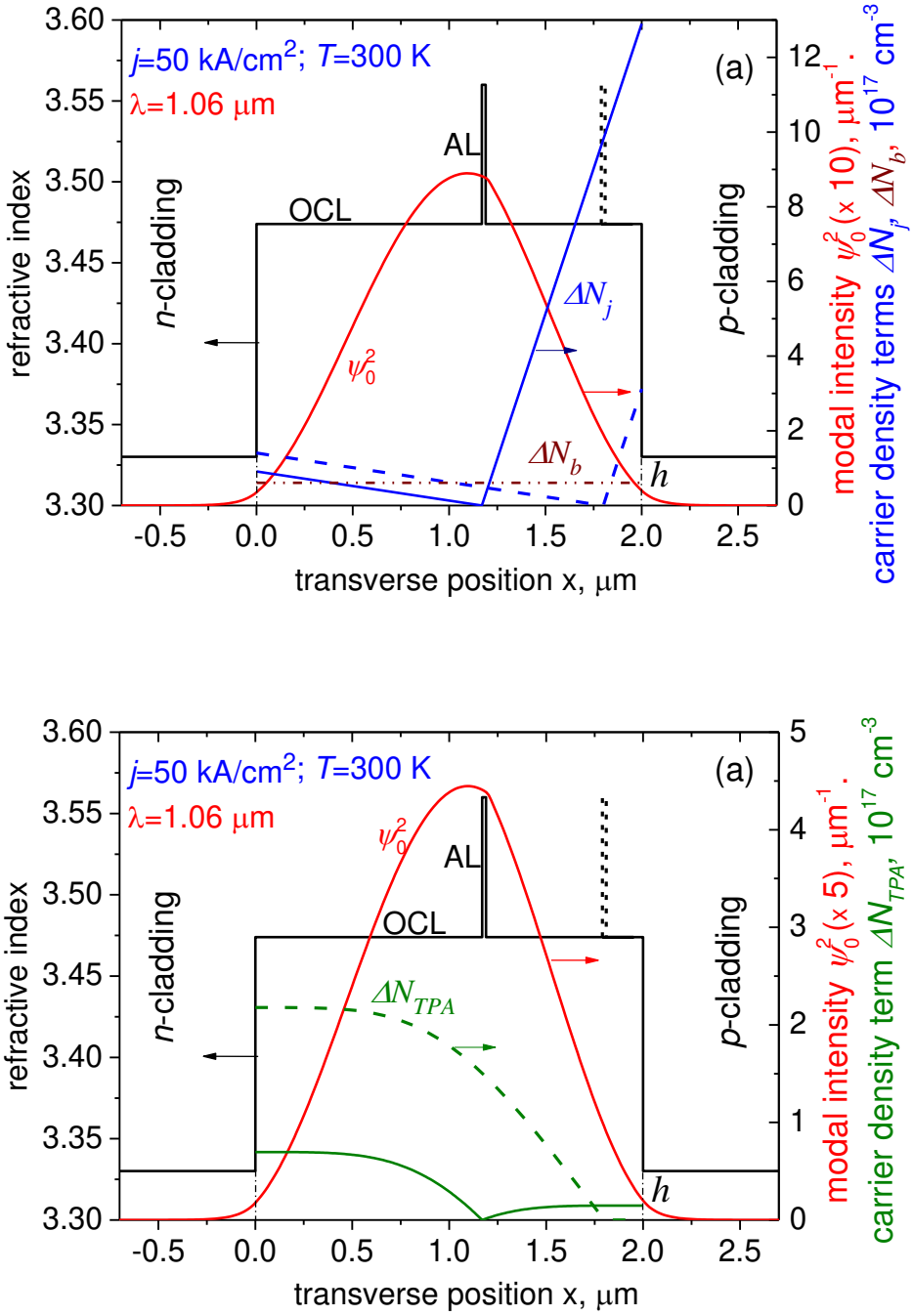
j=50 kA/cm2; T=300 K
λ=1.06 μm
(a)
AL
OCL
n-cladding
p-cladding
h
ΔNj
ψ02
ΔNb
refractive index
transverse position x, μm
modal intensity ψ02(x 10), μm-1 .
carrier density terms ΔNj, ΔNb, 1017 cm-3
ΔNTPA
ψ02(x 5), μm-1 .
carrier density term ΔNTPA, 1017 cm-3

Figure 3

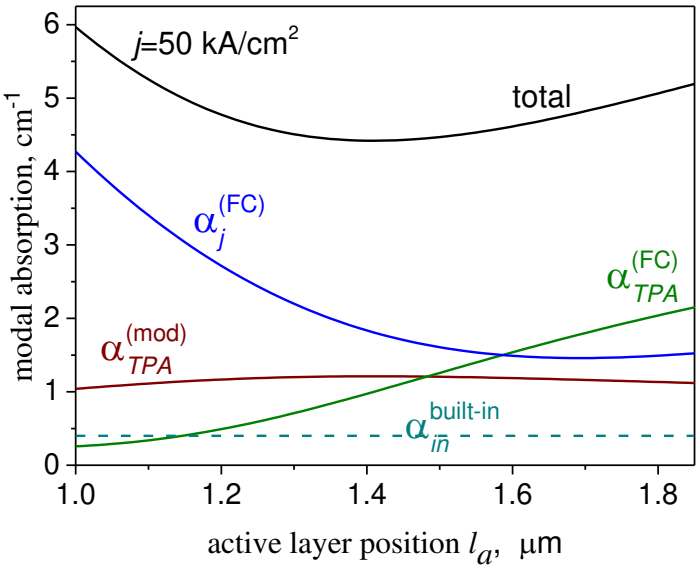
j=50 kA/cm2
total
α(FC) j
α(FC) TPA
α(mod) TPA
α built-in in
modal absorption, cm-1
active layer position la, μm
0
1
2
3
4
5
6
1.0
1.2
1.4
1.6
1.8

Figure 4

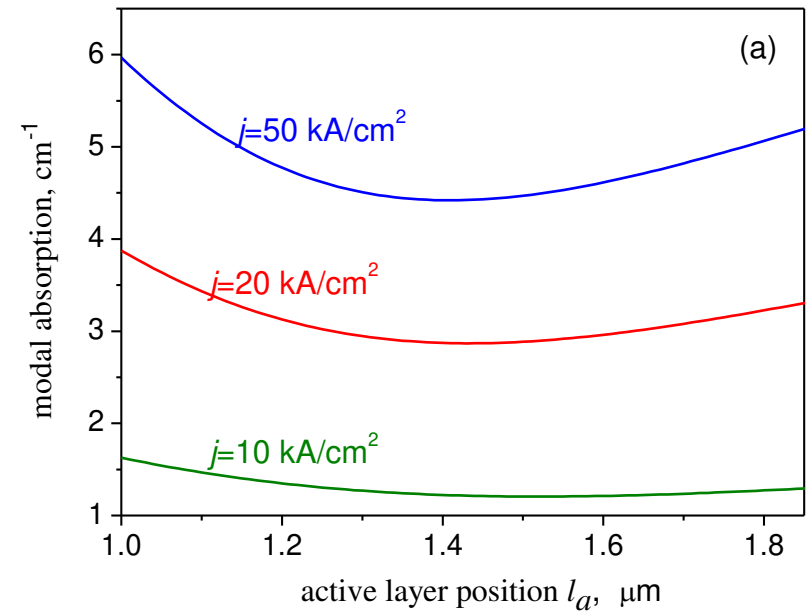
(a)
modal absorption, cm^{-1}
6
5
4
3
2
1
j=50 kA/cm^2
j=20 kA/cm^2
j=10 kA/cm^2
1.0
1.2
1.4
1.6
1.8
active layer position l_a, μm

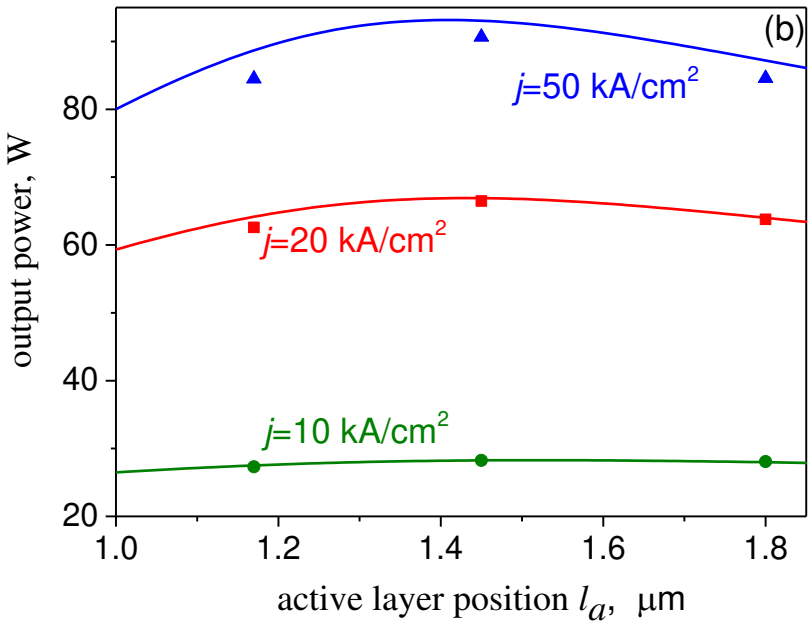
(b)
output power, W
80
60
40
20
j=50 kA/cm^2
j=20 kA/cm^2
j=10 kA/cm^2
1.0
1.2
1.4
1.6
1.8
active layer position l_a, μm

Figure 5

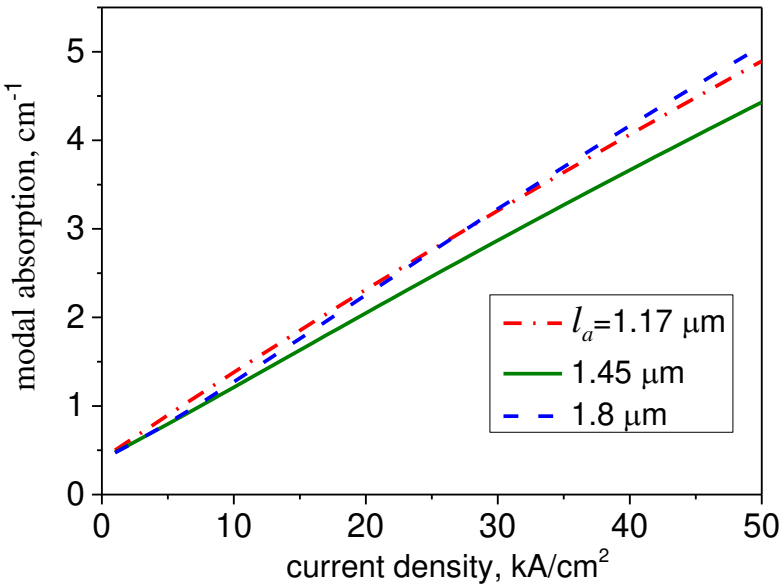
modal absorption, cm-1
current density, kA/cm2
0
1
2
3
4
5
0
10
20
30
40
50
la=1.17 μm
1.45 μm
1.8 μm

Figure 6

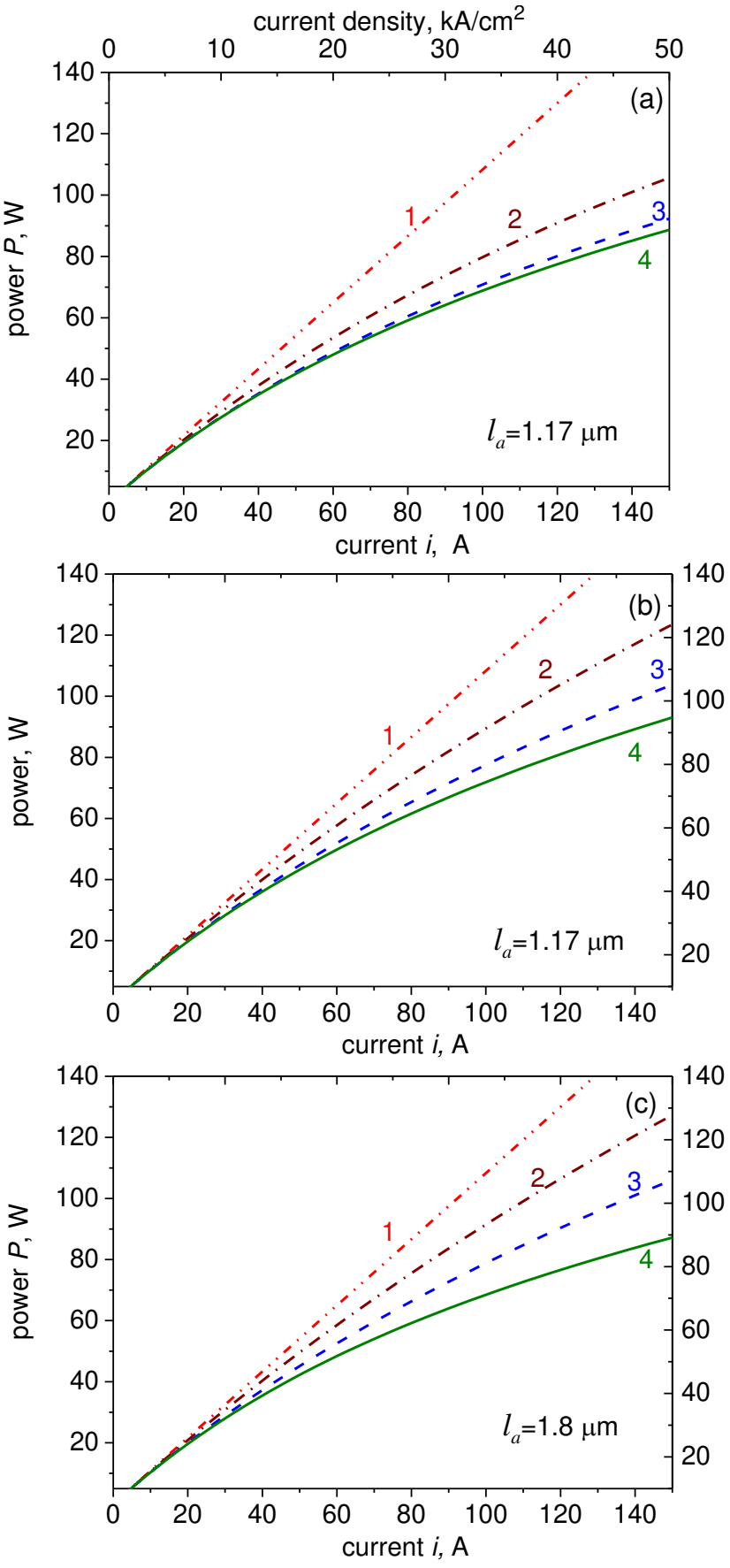
current density, kA/cm2
power P, W
(a)
1
2
3
4
la=1.17 μm
current i, A
power, W
(b)
la=1.17 μm
current i, A
power P, W
(c)
la=1.8 μm
current i, A

Figure7

References.

[1] I. S. Tarasov, "High-power semiconductor separate-confinement double heterostructure lasers," *Quantum Electronics,* vol. 40, pp. 661-681, 2010 2010.

[2] P. Crump, G. Erbert, H. Wenzel, C. Frevert, C. M. Schultz, K. H. Hasler*, et al.*, "Efficient High-Power Laser Diodes," *IEEE Journal of Selected Topics in Quantum Electronics,* vol. 19, Jul-Aug 2013.

[3] M. R. Gokhale, J. C. Dries, P. V. Studenkov, S. R. Forrest, and D. Z. Garbuzov, "High-power high-efficiency 0.98-mu m wavelength InGaAs-(In)GaAs(P)-InGaP broadened waveguide lasers grown by gas-source molecular beam epitaxy," *Ieee Journal of Quantum Electronics,* vol. 33, pp. 2266-2276, Dec 1997.

[4] A. Al-Muhanna, L. J. Mawst, D. Botez, D. Z. Garbuzov, R. U. Martinelli, and J. C. Connolly, "High-power (> 10 W) continuous-wave operation from 100-mu m-aperture 0.97-mu m-emitting Al-free diode lasers," *Applied Physics Letters,* vol. 73, pp. 1182-1184, Aug 1998.

[5] N. A. Pikhtin, S. O. Slipchenko, Z. N. Sokolova, A. L. Stankevich, D. A. Vinokurov, I. S. Tarasov*, et al.*, "16W continuous-wave output power from 100 mu m-aperture laser with quantum well asymmetric heterostructure," *Electronics Letters,* vol. 40, pp. 1413-1414, Oct 2004.

[6] D. A. Vinokurov, S. A. Zorina, V. A. Kapitonov, A. V. Murashova, D. N. Nikolaev, A. L. Stankevich*, et al.*, "High-power laser diodes based on asymmetric separate-confinement heterostructures," *Semiconductors,* vol. 39, pp. 370-373, Mar 2005.

[7] A. Knauer, G. Erbert, R. Staske, B. Sumpf, H. Wenzel, and M. Weyers, "High-power 808 nm lasers with a super-large optical cavity," *Semiconductor Science and Technology,* vol. 20, pp. 621-624, Jun 2005.

[8] L. Fan, C. S. Cao, G. Thaler, B. Caliva, I. Ai, S. Das*, et al.*, "Record High-Temperature Long-Pulse Operation of 8xx-nm Diode Laser Bar with Aluminum-Free Active Region," *Ieee Journal of Selected Topics in Quantum Electronics,* vol. 17, pp. 1727-1734, Nov-Dec 2011.

[9] P. W. Juodawlkis, J. J. Plant, W. Loh, L. J. Missaggia, F. J. O'Donnell, D. C. Oakley*, et al.*, "High-Power, Low-Noise 1.5-mu m Slab-Coupled Optical Waveguide (SCOW) Emitters: Physics, Devices, and

Applications," *Ieee Journal of Selected Topics in Quantum Electronics,* vol. 17, pp. 1698-1714, Nov-Dec 2011.

[10] B. Lanz, B. S. Ryvkin, E. A. Avrutin, and J. T. Kostamovaara, "Performance improvement by a saturable absorber in gain-switched asymmetric-waveguide laser diodes," *Optics Express,* vol. 21, pp. 29780-29791, Dec 2013.

[11] Y. Yamagata, Y. Yamada, M. Muto, S. Sato, R. Nogawa, A. Sakamoto*, et al.*, "915nm high power broad area laser diodes with ultra-small optical confinement based on Asymmetric Decoupled Confinement Heterostructure (ADCH)," in *High-Power Diode Laser Technology and Applications Xiii*. vol. 9348, M. S. Zediker, Ed., ed, 2015.

[12] K. H. Hasler, H. Wenzel, P. Crump, S. Knigge, A. Maasdorf, R. Platz*, et al.*, "Comparative theoretical and experimental studies of two designs of high-power diode lasers," *Semiconductor Science and Technology,* vol. 29, Apr 2014.

[13] M. Buda, T. G. vandeRoer, L. M. F. Kaufmann, G. Iordache, D. Cengher, D. Diaconescu*, et al.*, "Analysis of 6-nm AlGaAs SQW low-confinement laser structures for very high-power operation," *Ieee Journal of Selected Topics in Quantum Electronics,* vol. 3, pp. 173-179, Apr 1997.

[14] B. S. Ryvkin, E. A. Avrutin, and J. T. Kostamovaara, "Narrow versus broad asymmetric waveguides for single-mode high-power laser diodes," *Journal of Applied Physics,* vol. 114, Jul 2013.

[15] B. Ryvkin, E. A. Avrutin, and J. T. Kostamovaara, "Asymmetric-Waveguide Laser Diode for High-Power Optical Pulse Generation by Gain Switching," *Journal of Lightwave Technology,* vol. 27, pp. 2125-2131, Jun 2009.

[16] B. S. Ryvkin and E. A. Avrutin, "Asymmetric, nonbroadened large optical cavity waveguide structures for high-power long-wavelength semiconductor lasers," *Journal of Applied Physics,* vol. 97, Jun 2005.

[17] B. Ryvkin and E. Avrutin, "Non-uniform carrier accumulation in optical confinement layer as ultimate power limitation in ultra-high-power broad-waveguide pulsed InGaAs/GaAs/AlGaAs laser diodes," *Electronics Letters,* vol. 42, pp. 1283-1284, Oct 2006.

[18] D. Z. Garbuzov, A. V. Ovchinnikov, N. A. Pikhtin, Z. N. Sokolova, I. S. Tarasov, and V. B. Khalfin, "Experimental and theoretical investigations of singularities of the threshold and power characteristics of ingaasp/inp separate-confinement double-heterostructure lasers (lambda = 1.3 mu-m)," *Soviet Physics Semiconductors-USSR,* vol. 25, pp. 560-564, May 1991.

[19] B. Ryvkin and E. Avrutin, "Heating-induced carrier accumulation in the optical confinement layer and the output power in broadened symmetric and narrow asymmetric waveguide laser diodes," *Journal of Applied Physics,* vol. 101, Jun 2007.

[20] P. W. Juodawlkis, J. J. Plant, J. P. Donnelly, A. Motamedi, and E. P. Ippen, "Continuous-wave two-photon absorption in a Watt-class semiconductor optical amplifier," *Optics Express,* vol. 16, pp. 12387-12396, Aug 2008.

[21] A. R. Motamedi, J. J. Plant, J. P. Donnelly, P. W. Juodawlkis, and E. P. Ippen, "Ultrafast nonlinearities and gain dynamics in high-power semiconductor amplifiers," *Applied Physics Letters,* vol. 93, Dec 2008.

[22] M. Dogan, C. P. Michael, Y. Zheng, L. Zhu, and J. H. Jacob, "Two photon absorption in high power broad area laser diodes," *Proceedings of SPIE,* vol. 89650P, 2014.

[23] A. Demir, M. Peters, R. Duesterberg, V. Rossin, and E. Zucker, "Semiconductor Laser Power Enhancement by Control of Gain and Power Profiles," *Ieee Photonics Technology Letters,* vol. 27, pp. 2178-2181, Oct 15 2015.

[24] D. A. Veselov, N. A. Pikhtin, A. V. Lyutetskiy, D. N. Nikolaev, S. O. Slipchenko, Z. N. Sokolova*, et al.*, "Effect of laser cavity parameters on saturation of light-current characteristics of high-power pulsed lasers," *Quantum Electronics,* vol. 45, pp. 597-600, 2015.

[25] H. Kogelnik, "Theory of dielectric waveguides," in *Integrated Optics*, T. Tamir, Ed., ed Berlin – Heidelberg – New York: Springer-Verlag, 1975, pp. 15-79.

[26] B. S. Ryvkin and E. A. Avrutin, "Effect of carrier loss through waveguide layer recombination on the internal quantum efficiency in large-optical-cavity laser diodes," *Journal of Applied Physics,* vol. 97, Jun 2005.

[27] N. K. Dutta, "Calculated temperaure dependence of threshold current of GaAs-AlXGa1-XAs double heterostructure lasers," *Journal of Applied Physics,* vol. 52, pp. 70-73, 1981.

[28] C. Y. Tsai, C. Y. Tsai, Y. H. Lo, R. M. Spencer, and L. F. Eastman, "Nonlinear gain coefficients in semiconductor quantum-well lasers - effects of carrier diffusion, capture, and escape," *IEEE Journal of Selected Topics in Quantum Electronics,* vol. 1, pp. 316-330, Jun 1995.

[29] B. S. Ryvkin and E. A. Avrutin, "Spatial hole burning in high-power edge-emitting lasers: A simple analytical model and the effect on laser performance," *Journal of Applied Physics,* vol. 109, Feb 2011.

[30] H. Wenzel, "Basic Aspects of High-Power Semiconductor Laser Simulation," *IEEE Journal of Selected Topics in Quantum Electronics,* vol. 19, Sep-Oct 2013.

[31] E. A. Avrutin, B. S. Ryvkin, A. S. Payusov, A. A. Serin, and N. Y. Gordeev, "Fundamental transverse mode selection and self-stabilization in large optical cavity diode lasers under high injection current densities," *Semiconductor Science and Technology,* vol. 30, Nov 2015.